J Mater Sci: Mater Med (2010) 21:665–674
DOI 10.1007/s10856-009-3895-x

In vitro photothermal study of gold nanoshells functionalized with small targeting peptides to liver cancer cells

Shun-Ying Liu · Zhong-Shi Liang · Feng Gao · Shu-Fang Luo · Guo-Quan Lu

Received: 16 February 2009 / Accepted: 2 October 2009 / Published online: 16 October 2009

Abstract Gold nanoshells functionalized with a small peptide as a targeting agent were designed and synthesized for photothermal therapy of hepatocarcinoma. The nanoshells exhibited high absorption in the near-infrared (NIR) range, 800–1,100 nm, and were functionalized with 12-amino acid sequence peptides for targeting liver cancer cells. The nanoshells were characterized by Dynamic Light Scattering (DLS), Transmission Electron Microscope (TEM) and IR spectra. The functionalized gold nanoshells showed good targeting ability to liver cancer cells BEL-7404 and BEL-7402 while not to the normal healthy liver cell HL-7702, and also had a low cytotoxic activity. The fluorescence images showed that the gold nanoshells caused death to the liver cancer cells efficiently after being treated with a NIR light in vitro. These simple, stable, low cytotoxic, cancer-cell targeting gold nanoshells present a great promise as delivery agents for the selective photothermal treatment of liver cancer cells.

Electronic supplementary material The online version of this article (doi:10.1007/s10856-009-3895-x) contains supplementary material, which is available to authorized users.

S.-Y. Liu · Z.-S. Liang · F. Gao · S.-F. Luo (✉)
Advanced Research Center of NBIC Integrated Drug Discovery and Development, East China Normal University, Shanghai 200062, China
e-mail: sfluo@sist.ecnu.edu.cn

G.-Q. Lu
Department of Materials Science and Engineering, Virginia Polytechnic Institute and State University, Blacksburg, VA 24061, USA

1 Introduction

Hepatocarcinoma is one of the most common malignancies with a high mortality rate in the world [1]. For years, patients with the liver cancer have been treated by a number of therapeutic methods such as chemotherapy, radiation, Gene therapy, and liver transplantation as well as surgery. The therapeutic treatments have significant side effects [2, 3] because of the low selectivity of the therapeutic agents and gene therapy vectors to hepatocarcinoma at the cell level. And the surgical operation is costly, typically requires a long recovery time, and often has complications. On the other hand, thermal ablation therapies are minimal invasive alternatives to the mentioned treatments; they are relatively simple to perform and have the potential of improving recovery time, reducing complication rates and hospital stays. Recently, a laser-induced photothermal therapy has attracted much attention [4, 5] as a promising thermal treatment of cancers based on some metal nanoparticles, such as gold nanorod and nanoshells. This treatment utilizes metal nanoparticles as delivery agents of thermal energy since these nanoparticles have high optical absorption in the near-infrared (NIR) range (700–1,100 nm). Bhatia [6] has described an integrated approach to improve the photothermal therapy of long-circulating gold nanorod antennas with the guide of theoretical computation. Pioneered by Halas [7, 8] and the others, gold nanoshells have been successfully used as the delivery agents for photothermal therapy of some cancers.

Gold nanoshells, a new type of nanomaterials, are composed of a dielectric core (e.g., silica) coated by a nanometer-thick gold shell. The metallic nanoshells exhibit strong absorption to light by the excitation of plasmon resonance in the thin metallic films. Their absorption characteristics can be tailored by varying the ratio of core

diameter to metal shell thickness [9]. Their absorption property in the near infrared (NIR) region between 700 and 1,100 nm is particularly important for application in photothermal treatment because biological chromophores or water molecules do not absorb significantly within this spectral region. Thus, the NIR photons can penetrate deep into biological samples such as tissue or whole blood [10] and then to be absorbed in the localized regions where the metallic nanoshells are present. The absorbed light energy by the gold nanoshells is released as heat and transferred to the surrounding biological tissues. Gold nanoshells have been shown to be non-toxic and highly biocompatible [11] and the shell surface can readily be modified chemically for applications in the field of bioconjugation. The nanoshells have been shown to passively accumulate in tumors after intravenous injections [12], but this is mostly due to the leaky vasculature characteristic of tumors vessels [13]. For the therapy to be effective, the nanoshell surface needs to be functionalized with a targeting agent specific to the cancer cells. By functionalizing with target specific antibodies, gold nanoshells were shown to enhance the visualization of the targeted imaging of HER2-positive breast cancer cells [14] as well as to confirm the capability of targeted photothermal ablation of tumor cells [15]. The potential of surface-modified gold nanoshells have been demonstrated for cancer-targeted imaging [16] and therapy [17]. But, the photothermal treatment of hepatocarcinoma using gold nanoshells functionalized with a targeting agent to liver cancer cells has not been demonstrated.

Many attempts have been tried to develop targeting drugs or imaging agents for cancers such as hepatocarcinomas through the identification of a specific targeting unit, such as antibodies [14], folic acid [18] and galactose [19]. However, the immunogenicity of these targeting units to human body and the penetration to tumor tissues are difficult to determine, thus still wait to be fully solved. Because of their low immunogenicity and high biocompatibility as well as strong penetration into tissues, peptides with short amino acid sequences based on the phage display technology [20] have attracted much attention in the targeting therapeutic field. Recently, through a cell-based ELISA, immunofluorescence and in vivo binding study, Qian et al. [21] demonstrated that a short peptide with the sequence of AGKGTPSLETTP (A54) was most effective in targeting four kinds of human liver cancer cell lines (BEL-7404, BEL-7402, SMMC-7721, and HepG2), and was ineffective to the normal liver cell line HL-7702. These findings suggest a promising application of the A54 peptide in targeting treatment of liver cancer.

In this paper, we report the synthesis of uniform-sized gold nanoshells with surface functionalized by the A54 peptide via cysteine linkers. These A54 functionalized nanoshells (A54-nanoshells) were characterized by UV–vis, IR, DLS, and TEM. The effectiveness and selectivity of the targeting property of these A54-nanoshells towards BEL-7404 and BEL-7402 liver cancer cells were determined from in vitro photothermal treatment. The increased efficiency obtained in this study clearly demonstrates the potential of the photothermal therapeutic method that utilizes the A54-peptide functionalized gold nanoshells for effective treatment of hepatocarcinoma. To the best of our knowledge, this is the first report on a targeting gold nanoshell to liver cancer cells with a small peptide as a targeting group.

2 Materials and methods

2.1 Materials

Most of the chemical reagents were purchased from Sigma–Aldrich and used as received. They are: 3-aminopropyl triethoxysilane (APTES, 99%), tetraethyl orthosilicate (TEOS, 99.999%), tetrakis (hydroxymethyl) phosphonium chloride (THPC, 80%), ammonium hydroxide (NH_4OH, 25%), formaldehyde (HCHO, 37%), hydrogen tetrachloroaurate (III) hydrate ($HAuCl_4$, 99.99%), potassium carbonate (K_2CO_3, $\geq$99.0%), absolute ethanol (EtOH, 99.5%), sodium hydroxide (NaOH, AR), thiazolyl blue formazan (MTT, powder), propidium iodide (PI, >95%), and acridine orange (AO, dye content 90%).

The human hepatocellular carcinoma cell line BEL-7404, BEL-7402 and normal liver cell line HL-7702 were purchased from the cell bank of Shanghai Institute for Biological Science (Shanghai, China); Calcium chloride ($CaCl_2$, AR) was obtained from Sinopharm Chemical Reagent Co., Ltd. (Shanghai, China); RPMI 1640 culture medium was purchased from GIBCO (Grandisland, NY, USA); Ttrypsin (1:250) powder was bought from Invitrogen (USA). Streptomycin/ampicillin solution and fetal bovine serum (FBS) were purchased from Every Green Organism Engineering Materials Co., Ltd. (USA). CAGKGTPSLETTP peptide (C-A54) was synthesized by HD Biosciences Ltd. (Shanghai, China). Deionized (DI) water was used at every stage of reaction and washing. The aqueous solutions of K_2CO_3 and NaOH were filtered through a filter membrane of 0.2 μm pore size (PN4612, PALL Corporation, USA) before using. All the glass vessels were dipped in aqua regia overnight and washed with DI water before using.

The zeta-potential and size distributions of all particles were measured by a dynamic light scattering (DLS) potentiometer (Zetasizer Nano ZS, Malvern, UK). The value of the size distribution was given as the Polydistribution Index (PdI) at pH = 6.5. The elemental composition of the material was analyzed by an energy-dispersive X-ray

analysis spectrometer (Oxford-IMCA). The FTIR data were collected on a Nicolet NEXUS 670 spectrometer with the samples in KBr. The Raman data were investigated by a Nicolet MAGNA 560 E.S.P. spectrometer equipped with a Raman module, and samples were dispersed in water and subjected to 100 scans at a spectral resolution of 4 cm^{-1}. The plasmon absorption peak was recorded by UV–vis spectroscopy (YaYan 1900PC). The total amounts of the gold nanoshells absorbed or uptake by the cells were collected by the Inductive Coupled Plasma (ICP) Emission Spectrometer (Varian 710ES, USA).

2.2 Preparation of gold nanoshells

Generally, the gold nanoshells were synthesized based on the modified of Halas [22]. Initially, silica spheres were made through the base-catalyzed hydrolysis of TEOS by the Stöber's method [23]. A 3.0 ml volume of ammonium solution (25%) was used as a catalyst in the formation of the colloidal silica particles. Then, 0.2 ml of TEOS solution was added to 50 ml of ethanol solution and stirred overnight. The mixture was then centrifuged and the separated solid was redispersed in 10 ml of EtOH.

An excess of APTES (300 μl) was added to the solution (10 ml) of silica core particles with vigorous stirring for 2 h. To enhance the covalent bonding of the APTES groups to the silica surface, the solution was diluted to 100 ml and gently stirred at 70°C for 1 h. After several centrifugations, the APTES–SiO_2 was redispersed in 10 ml of EtOH.

To prepare gold colloids (GC) of 1–3 nm size, 1.5 ml of 0.2 M NaOH and 1.0 ml of 0.96% THPC were mixed with 45 ml of DI water, and 2.0 ml of 25 mM $HAuCl_4$ was added quickly to the mixed solution [24]. The colloid solution was filtered after 0.5–2 h. The filtered solution was stored in a refrigerator maintained at 4°C for 5–30 days and then concentrated using a rotary evaporator.

For the fabrication of the seed particles (gold attached to the silica core particles), 3.0 ml of APTES–SiO_2 was added to the concentrated gold colloids (20 ml) and mixed thoroughly. The resulting seed particles were washed by centrifugation and redispersed in an ultrasonic bath in 10 ml of water for the next step.

The growth of the gold nanoshell layer on the seed particles was conducted by subsequent deposition and reduction of Au^{3+} by formaldehyde. To do so, a solution of 25 mg of anhydrous potassium carbonate was added to 100 ml of DI water containing 1.5 ml of 25 mM $HAuCl_4$ solution. This solution is called PCG in short. The PCG solution was stocked at 4°C in dark for one day. Then 40 ml of PCG were rapidly stirred with 1 ml of the seed solution followed by the addition of the diluted aqueous formaldehyde solution (2%, 2 ml) to form the gold nanoshells. After stirring for 30 min, the mixture was then centrifuged and the separated solid was redispersed in DI water. This purifying procedure was repeated for three times. The final separated solid was redispersed in 1.5 ml of DI water to obtain a final nanoshell concentration of 3.0×10^{11} particles/ml.

2.3 Preparation of the Cys-conjugated A54-functionalized gold nanoshells (A54-nanoshells)

The Cys-conjugated A54 peptide (5 mg/ml) was added to the nanosehlls (3.0×10^9 nanoshells/ml, absorption = 1.2 at 800 nm at 1 cm path length) to obtain a final A54 concentration of 500 μg/ml. The suspension was reacted at 4°C overnight and the non-reacted peptide was removed by centrifugation at 1,500 rpm for several times. Then, the resulting particles (A54-nanoshells) were redispersed in 1.5 ml of RPMI 1640 medium without fetal bovine serum (FBS) and antibiotics to obtain a final nanoshell concentration of 3.0×10^{11} particles/ml (absorption = 3.8 at 800 nm at a 1 cm path length).

2.4 Thermogravimetric analysis

The thermal gravimetric analysis was determined on the TGA/SDTA 851 Mettler-Toledo Instrument under a stream of nitrogen, at a heating rate of 3°C/min. The number of A54 on the surface of the gold nanoshell was determined by thermogravimetric analysis and calculated by:

$$N_P = \frac{(P_M - P_N) \times M_M}{W \times N_N} \quad (1)$$

where N_P, N_N, P_M, P_N, M_M are the molecular number of the Cys-conjuagted A54 peptide per nanoshell, the number of the A54-nanoshells, the weight loss ratio of the A54-nanoshells, the weight loss ratio of the nanoshells free from A54 and the mass of the A54-nanoshells, respectively, and W is the molecular weight of the Cys-conjugated A54 peptide. Both the gold nanoshells and the A54-nanoshells were investigated by TGA.

2.5 Cell culture

BEL-7404, BEL7402 and the normal liver cell HL-7702 were cultured in RPMI 1640/10% FBS at 37°C in a humidified atmosphere containing 5% CO_2, and plated into 96-well or 12-well plates the day before use.

2.6 MTT assay

For cell viability test, optical density was determined at 570 nm using an automatic BIO-TEK reader (Powerwave XS, USA). Shortly, the cells were all digested with 0.1% trypsin, resuspended in serum containing medium RPMI

1640. Then the cells were plated (1×10^4 cells per well) in a 96-well microtiter plate (Corning, USA) and grown in 100 μl of RPMI 1640 culture medium with 10% FBS and 1% antibiotics. Following overnight incubation at 37°C in 5% CO_2 humidified atmosphere, the cells were treated with gold nanoshells (3.0×10^{10}, 6.0×10^9, 1.2×10^9, 2.4×10^8, 4.8×10^7, 9.6×10^6, 1.9×10^6, 3.8×10^5 particles/ml, respectively) for 48 h. At the end of incubation, the culture medium was replaced by 100 μl of MTT solution (0.5 mg/ml). After 4 h incubation at 37°C, 100 μl of dimethyl sulfoxide (DMSO) was added to each well to replace the culture medium and dissolve the insoluble formazan-containing crystals. Optical density was determined using an automatic reader. Cell viability was calculated in reference to cells incubated with culture medium alone. The experiment was repeated three times.

2.7 FACS experiment

For analysis of cell proliferation, about 10^6 Cells were incubated with the A54-nanoshells (3.0×10^{10} particles/ml) for 48 h. The cell group without the A54-nanoshells was also used as a control group. Cells were digested with 0.1% trypsin and washed with PBS (pH = 7.4) twice by centrifugation for 3 min at 1,000 rpm. The cells were continuatively fixed by 70% ethanol solution (2 ml) for 12 h at 4°C. After washing with PBS by centrifugation, the cells were resuspended in 0.5 ml of PBS. Then, 0.5 ml of RNaseA deactivated in high temperature was added and the final concentration was 500 μg/ml. Subsequently, the above cell solution were stained with 1 ml of PI (100 μg/ml) and stood in dark for 15 min. Samples of coelomocytes were analyzed with a FACScalibur flow cytometer. 10,000 threshold events per worm sample were collected for cell composition or cell cycle, respectively. The results of the analysis were based on their FL2 fluorescence (emission at 585 nm, excitation at 488 nm) using Cellquest 7.0 software.

2.8 Fluorescence images

The free gold nanoshells or the A54-nanoshells were diluted with RPMI 1640 medium (free of FBS and antibiotics to eliminate the nonspecific interaction with the nanoshells) to get a final concentration of 3.0×10^{10} particles/ml. BEL-7404, BEL-7402 and HL-7702 cells were grown on cover-slips in a 12-well chamber culture plate with 3.0×10^5, 4.5×10^5 and 6.0×10^5 cells per well in 3.0 ml of RPMI 1640, respectively, containing 10% of FBS and 1% of antibiotics. After overnight incubation at 37°C in 5% CO_2 humidified atmosphere, the culture medium was replaced by 3.0 ml of the gold nanoshell or the A54-nanoshell solution (3.0×10^{10} particles/ml, free of FBS and antibiotics to eliminate the nonspecific interaction with the nanoshells) and the cultural process continued for 1 h. Following removing the medium and washing with PBS to remove the unbound nanoparticles, the cells were exposed to an NIR irradiation for 7 min and continued to incubate with RPMI 1640 medium (containing FBS and antibiotics) for 12 h. Then the irradiated cells were rinsed with PBS to remove the dead cells. Finally, the staining procedures were carried out and the stained cells were imaged under a darkfield microscope sensitive to scattered light. Images were taken with a Motic AE31 microscope equipped with a cooled frame CCD camera with excitation and emission wavelengths of 490 and 520 nm, respectively. All images were taken at the same magnification under the same lighting conditions.

2.9 TEM images

2.9.1 Nanoparticle samples prepared for TEM analysis

A drop of each solution was placed on Formavar + C-coated Cu TEM grids and air-dried at 25°C. The average size of the particles was also determined from the TEM images. When the particles in the TEM photos did not exhibit a clear boundary, a spherical boundary enclosing the particle was drawn on screen and used to calculate the size. The TEM images of the nanoparticles was obtained with a Philips CM 120 transmission electron microscope, working at a 60-kV accelerating voltage, and the high-resolution TEM image was obtained on a JEOL-JEM2100F transmission electron microscope, working at a 200-kV accelerating voltage.

2.9.2 Cells samples prepared for TEM analysis

Cells incubated with gold nanoshells were washed with phosphate buffered saline (PBS) three times, then the cells were digested by using 0.1% trypsin and fixed with 2% glutaraldehyde for 3 h. Then the cells were post-fixed in 1% osmium tetraoxide for 2 h, washed and dehydrated in graded concentrations of ethanol (25, 50, 70, and 100%) and propylene oxide. Then the cell samples were embedded in Epon and thin sections. Thin sections of 50 μm were collected on copper grids and stained with a lead citrate. The grids were observed using a JEM-2100 TEM (Hitachi Corp., Japan).

3 Results and discussion

3.1 Fabrication of the nanoshells and A54-nanoshells

It has been demonstrated that macromolecules and small particles in the 60–400 nm size range tend to extravasate

and accumulate in tumors via the "enhanced permeability and retention" (EPR) effect [25–28]. Therefore, we aimed at designing the diameter of our targeting gold nanoshells to be between 150 and 200 nm. Based on the Mie theory [25] on plasmon resonance of metal nanoparticles, and to ensure that the maximum optical absorption of the nanoshells was within the near infrared region, we chose silica particles with a diameter of ~140 nm as the dielectric core to construct gold nanoshells with gold shell thickness of ~20 nm.

Silica cores were grown using the modified Stöber [23] process which was based on the simple reduction of tetraethyl orthosilicate in ethanol. The resultant silica particles were examined under TEM and DLS. The particles shown in Fig. 1a had a narrow size distribution with a polydistribution index (PdI) of 0.01. The silica particles were reacted with 3-aminopropyltriethoxysilane (APTES) to introduce amine groups on the surface. Small gold colloids (1–3 nm) were then adsorbed to the silica surface. The adsorbed gold colloids were used as nucleation sites for the growth of additional gold that was reduced from the solution. This process continued until a thin layer of gold in nanometer scale was formed. The final gold nanoshell concentration was about 3.0×10^{11} particles/ml. The gold nanoshells were examined by TEM (Fig. 1b) and their optical absorption profiles were characterized by UV–vis spectroscopy (Fig. 2). DLS showed the PdI value of these nanoshells was 0.012, indicating a good monodispersity.

To attach the targeting peptide A54 to the nanoshell surface, cysteine (Cys), an amino acid with a mercapto group (SH) was introduced at the T-end of A54 by solid phase synthesis (C-A54). Subsequently, the Cys-conjugated A54 (5 mg/ml) was anchored to the nanoshells (3.0×10^9 nanoshells/ml, absorption = 1.2 at 800 nm at 1 cm path length) to obtain a final A54 concentration

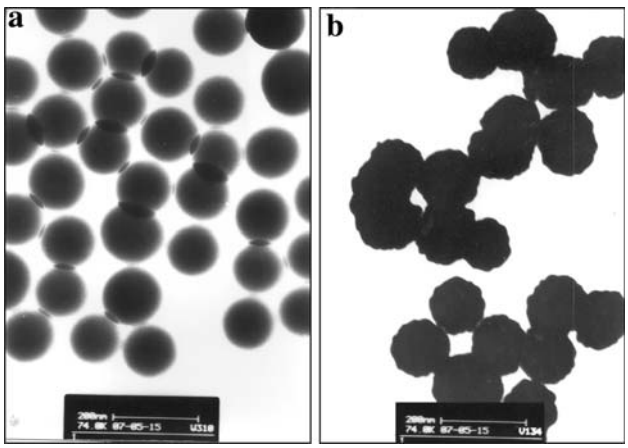

Fig. 1 TEM images of **a** silica particles with a diameter of ~140 nm; and **b** gold nanoshells capping the silica particles. The shell thickness is ~20 nm

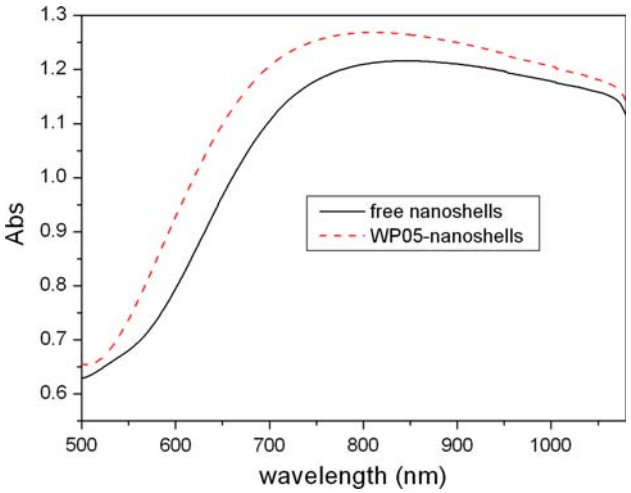

Fig. 2 UV–vis spectra of the free gold nanoshells (3.0×10^9 particles/ml, *black line*) and the A54-nanoshells (3.0×10^9 particles/ml, *red line*) in deionized water. (Color figure online)

of 500 μg/ml. The suspension was reacted at 4°C overnight and the non-reacted peptides were removed by centrifugation. Then, the resulting particles (A54-nanoshells) were redispersed in 1.5 ml of RPMI 1640 medium without FBS and antibiotics to obtain a final nanoshell concentration of 3.0×10^{11} particles/ml. The A54-nanoshell solution was much more stable than the free gold nanoshell solution and could be more easily redispersed in an ultrasonic bath. The absorption spectrum of the A54-nanoshells was shown in Fig. 2. The absorption intensity of the A54-nanoshells was slightly stronger than that of the free gold nanoshells at the same concentration in pure deionized water. In addition, the zeta potential of the nanoshells was decreased from −30 to −40 mV (in deionized water, pH = 6.5) after being coated with the Cys-conjugated A54, which demonstrated that the A54-nanoshells were more stable than the free gold nanoshells in water.

Figure 3 shows the FT-IR spectra of the gold nanoshells, the A54-nanoshells and the Cys-conjugated A54. The weak peak at 2,600 cm^{-1} (KBr) was attributed to the bending vibration of the mercapto group in the Cys-conjugated A54 which was much weaker than that was reported in the literature [22]. This is because that the SH groups are very unstable and can be easily oxidized to form S–S bonds between the two molecules containing SH groups [29]. However, both SH groups and S–S groups are readily to form Au–S bonds with gold [30, 31]. The oxidation of some SH groups seems to have no notable effect on the binding of the Cys-conjugared A54 to the surface of the gold nanoshells in our procedure. After the Cys-conjugated A54 was attached to the gold nanoshells, the weak peak of the mercapto groups disappeared completely. The observable C–H stretching bands at ca. 2,900 cm^{-1} and N–H bending bands at ca. 3,400 cm^{-1} indicated that the

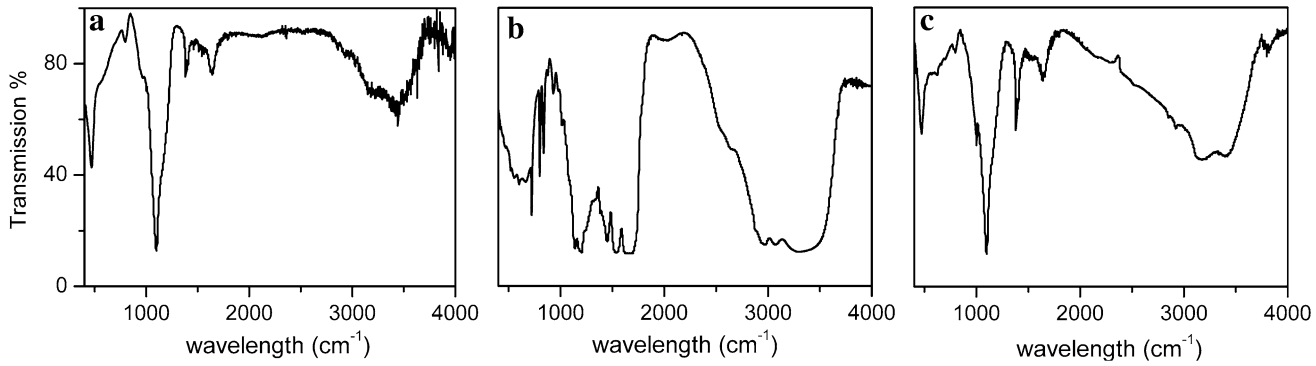

Fig. 3 FT-IR spectra of **a** the gold nanoshells, **b** the Cys-conjugated A54 peptide, and **c** the A54-nanoshells

Cys-conjugated A54 had been bound to the surface of the gold nanoshells through the formation of Au–S bonds.

The Raman spectra of the A54-nanoshells also indicated that the A54 had been successfully bound to the surface of the gold nanoshells (see the supporting information). The three bands in the Raman spectrum of the free Cys-conjugated peptide A54 were, respectively, attributed to ν(C–S) = 760 cm^{-1}, ν (C–C) = 1,120 cm^{-1}, and ν (C=O) = 1,700 cm^{-1}. These bands were also observed in the Raman spectrum of the A54-nanoshells. Similarly, no typical S–H bands exhibited at ca. 2,600 cm^{-1} in the Raman spectrum of the Cys-conjugated A54 [22], and this observation was consistent with the results of the FTIR spectra as explained above. The binding of A54 to the gold nanoshells was further confirmed by high-resolution TEM images (see the supporting information), which the surface of the functionalized particles became smoother after binding with the peptide.

Thermogravimetric analysis (TGA) is widely used to quantify the weight loss of some labile surface groups [32, 33]. To quantify the number of A54 on the surface of the gold nanoshells, both the gold nanoshells and the A54-nanoshells were investigated by TGA. The weight loss of the A54-nanoshells was ca. 4.0% and that of the gold nanoshells was ca. 1.37% within the temperature range of 150–600°C (data not shown). According to the weight of the gold nanoshell (which was calculated from the density of the material and the radius of the nanoparticles), the number of peptide on the surface of the gold nanoshell is about 3 × 10^3 molecules per gold nanoshell by calculation.

3.2 In vitro photothermal study of the A54-nanoshells

The cytotoxicity of the A54-nanoshells to inhibit cell growth was firstly determined by evaluating the livability of tumor cells (BEL-7404 and BEL-7402) using a MTT test, which is based on colorimetric determination of MTT being converted to formazan by viable cells. At any given concentration of the A54-nanoshells, both BEL-7404 and BEL-7402 presented a high cell viability (almost 100%, $P < 0.05$, $n = 6$), which suggested that the A54-nanoshells have a high biocompatibility and a low cytotoxicity.

Another method of determining the cytotoxicity of the nanoshells is to use flow cytometry (FCM), a routine technique now [34]. BEL-7402 cells were incubated with the A54-nanoshells (3.0 × 10^{10} particles/ml) for 24 h. The cell group without the A54-nanoshells was also used as a control group. For analysis of cell proliferation, samples were stained with propidium iodide (PI) according to [21] after centrifugation for 3 min at 1,000 rpm at 4°C. Figure 4

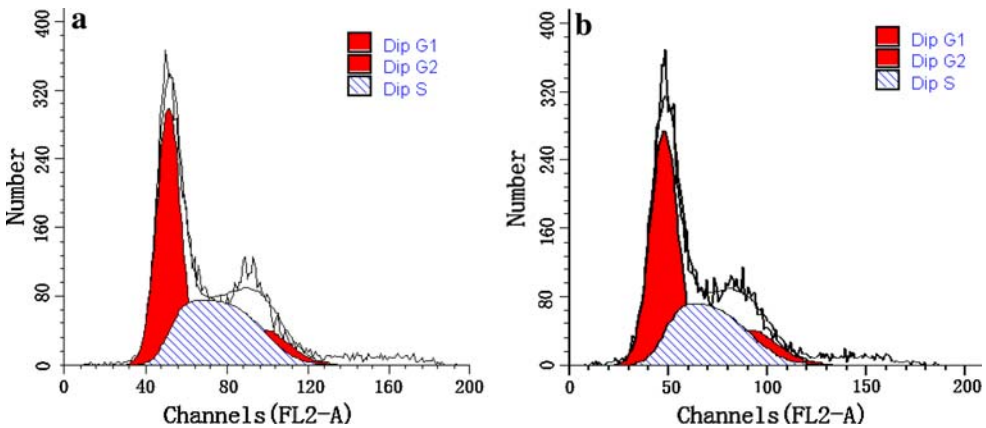

Fig. 4 Analyses of flow cytometry based on the FL2 fluorescence (emission at 585 nm, excitation at 488 nm) using Cellquest 7.0 software. Cells were stained with propidium iodide (PI). **a** BEL-7402 cells were incubated with the A54-nanoshells (3.0 × 10^{10} particles/ml) for 24 h; **b** BEL-7402 cells were incubated without the A54-nanoshells for 24 h

is the results of the analysis on the basis of their FL2 fluorescence (emission at 585 nm, excitation at 488 nm) using Cellquest 7.0 software. The diploid of the treated group in the G1, G2 and S phase of the cell cycle were 48.19, 12.86 and 38.95%, respectively. Similarly, the diploid of the controlled group were 50.66, 15.11 and 34.23%. The G1/G2 value of the treated group and the controlled group were 1.92 and 1.91, which indicated that the cells both in the treated and in the control groups grew normally. At the same time, no peak of cell apoptosis was observed before the G1 phase both in the treated and in the controlled groups. These results indicated that the A54-nanoshells had no effect on the diploid (or DNA) in the cell growth and had a high biocompatibility with the cells. The similar analytical results were obtained when treating BEL-7404 liver cancer cells with the A54-nanoshells (see the supporting information).

The in vitro photothermal study of the A54-nanoshells targeting towards liver cells was conducted by fluorescence microscopy [35–37]. Figure 5 shows the results of photothermal study of the free nanoshells and the A54-nanoshells. Their ability to target and cause the death of liver cancer cells (BEL-7404) under a NIR light irradiation was expressed in the fluorescence images. Dead cells were removed through washing after NIR irradiation and further incubation. Cells survived usually showed bright green fluorescence. In Fig. 5, the top three samples were not exposed to NIR light while the bottom samples were under a NIR light irradiation for 7 min. The samples in the left column were incubated without any nanoshells, no cell mortality was found even after being exposed to a NIR light, and so the fluorescence intensity of these two samples did not change. The samples in the middle column were incubated with the gold nanoshells, only a small fraction of the cells were found dead. However, after the cells were incubated with the A54-nanoshells and exposed to a NIR light, significant cell death occurred, and almost no fluorescence was observed (bottom row, right column). Also from these fluorescence images, an increased scatter-based optical contrast was observed from the cells treated with both the gold nanoshells (top row, middle column) and the A54-nanoshells (top row, right column), as compared to the control sample (top row, left column). This can be explained by the non-specific interaction between the nanoshells with the cells and the specific interaction (target-based binding) between the cells and the A54-nanoshells. This effect was also observed by other researchers [14]. The death of these cells was a result of increased temperature caused by the nanoshells that were bound to the cell surfaces or uptake by the cell after being exposed to a NIR light. All these results suggested that A54-nanoshells had a high targeting (binding) ability to the liver cancer cells because of the attached small peptide A54, which could significantly increase the efficiency of photothermal treatment. The similar observations were obtained when BEL-7402 liver cancer cells were tested under the same conditions (see the supporting information).

To further illustrate the targeting property of the A54-nanoshells to the hepatocarcinoma cells (BEL-7404 and BEL-7402) while not to the normal healthy liver cells (HL-7702), the three cell lines were, respectively, incubated with the A54-nanoshells on coverslips and later exposed to the NIR laser for 7 min under the same conditions. The control groups without the A54-nanoshells were also treated with the NIR laser. Figure 6 shows the fluorescence images of these cells after being exposed to a NIR irradiation. Compared to the normal liver cells HL-7702, cancer cells BEL-7404 and BEL-7402 exhibited a significant cell death after being treated with the NIR laser (bottom row, left and middle column). However, HL-7702 did not show any visible cell death from the fluorescence image even after being incubated with the

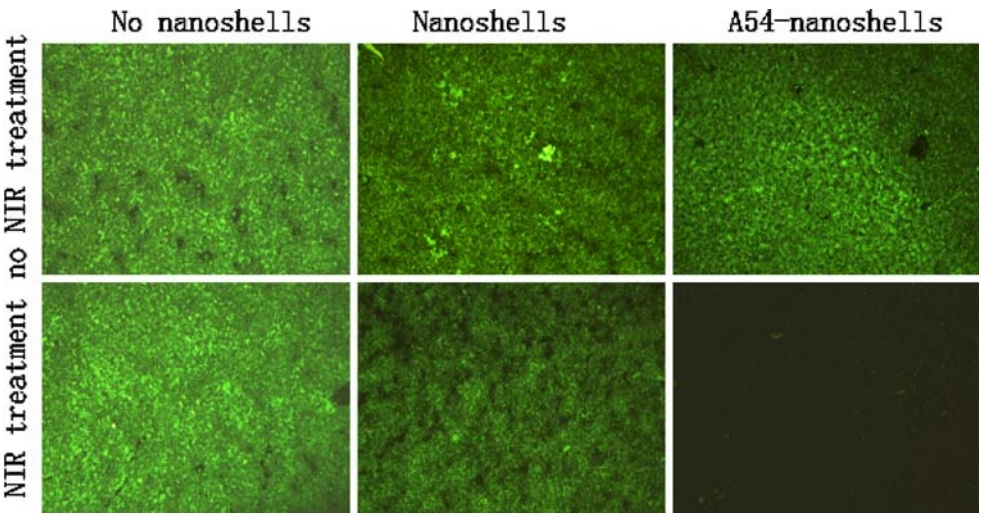

Fig. 5 Fluorescence images of BEL-7404 liver cancer cells. Cells were treated with the gold nanoshells (*middle column*, 3.0×10^{10} particles/ml), the A54-nanoshells (*right column*, 3.0×10^{10} particles/ml) and without any nanoshells (*left column*). The bottom groups were exposed to a NIR laser for 7 min and the top groups (control groups) were not. Cell viability was assessed via acridine orange staining

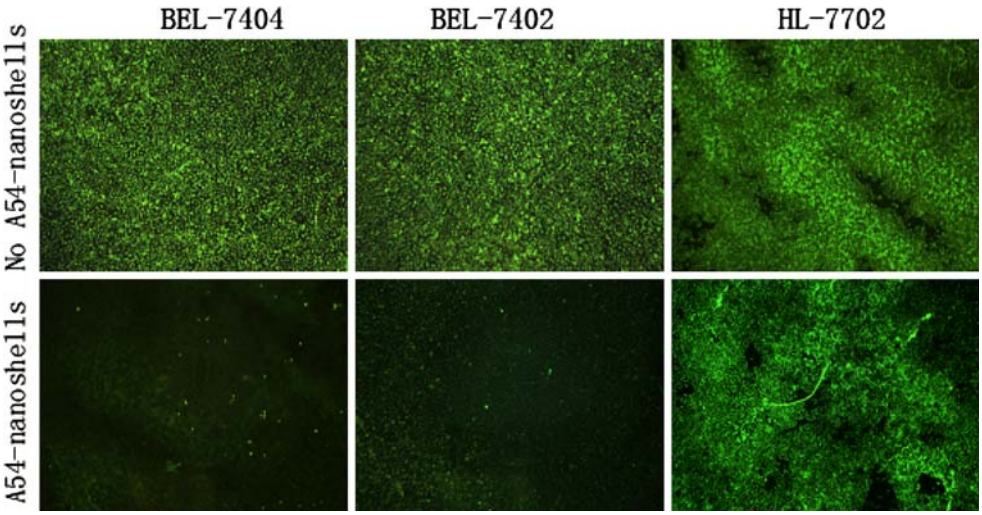

Fig. 6 Fluorescence images of the liver cancer cells BEL-7404 (*left column*), BEL-7402 (*middle column*) and the normal healthy liver cells HL-7702 (*right column*) incubated with (*bottom row*) and without (*top row*) the A54-nanoshells (3.0×10^{10} particles/ml) after being treated with a NIR light for 7 min. Cell viability was assessed via acridine orange staining

A54-nanoshells and subsequently exposed to the NIR laser (bottom row, right column). For the control groups (top row), neither the cancer cells nor the normal cells expressed an observable cell death (no obvious fluorescence intensity change). These observations further confirmed that the A54-nanoshells possessed a good targeting ability to both BEL-7404 and -7402 liver cancer cells in our study. This targeting property can significantly increase the efficiency of the photothermal destruction of the cancer cells. This result also implied that the A54 peptide remained its targeting activity after being modified and bound to the surface of the gold nanoshells.

To further investigate how the cancer cells were destroyed by photothermal treatment in the presence of the A54-nanoshells, the cancer cells were incubated with the A54-nanoshells for 1, 6, 12 and 24 h, respectively, and then observed under a microscope and TEM. The cells that were incubated for 24 h were also treated with a NIR light for 1, 3 and 5 min, respectively. After one-hour incubation with the A54-nanoshells, the color of BEL-7402 and BEL-7404 cells were turned to black observable by naked eyes as well as a microscope. This was due to the accumulation of the A54-nonoshells (black color) on the cells. Progressive TEM images showed that a very small amount of the A54-nanoshells on the cell (BEL-7402) surface was slowly internalized with time, and the amount of the uptake reached the maximum after 24 h within this time frame (data not shown). At this point, the cytoplasm of BEL-7402 still showed numerous normal organelles including endoplasmic reticulum, mitochondria and lysosomes. Abundant microvilli were seen on the surface and the nucleus was observable in the lower-middle part (Fig. 7a). But when the cells were treated with the NIR light for 1 min, most organelles in the cytoplasm had changed their appearance or disappeared (Fig. 7b). The cell volume also had shrunk obviously, which might indicate the injury of the cell. But a few microvilli were still seen on the cell surface and the nucleus contained a nucleolus was also observed. While after treating the cells for additional 2 min (total of 3 min), almost all the microvilli disappeared (Fig. 7c). When the cells were treated with the light for 5 min total, some blebs appeared in the cytoplasm of the cells, indicating severe cell injury that was caused by the increased temperature (Fig. 7d). At the same time the volume of the cell was further decreased. Here, the TEM results indicated that the cancer cells could be killed by photothermal treatment which could lead to dramatic cell shape change and thus the function. In an in vitro study done by Malini Olivo et al. [38], cell viability was measured in photothermal therapy, photodynamic therapy as well as combined method of the two. They concluded that cell viability was related to the dose of the light, the irradiation time and the concentration of the nanoshells. Combining photodynamic therapy with photothermal therapy led to further destruction of the cells, thus the increased cancer treatment efficiency.

Other previous studies demonstrated that cancer cells could be destroyed through DNA damage, glucose deprivation etc. [39, 40] when the temperature was increased to 43°C. In our study, only cell morphology was studied with a NIR light exposure of up to 5 min. Although the actual temperature could not be determined experimentally with our current setup, dramatic change in cell morphology was obvious and that was the cause from raising the temperature in the cells with the nanoshells. DNA damage or other facts contributing to the cell death could happen during this process and our flow cytometry experiment (data not shown) indicated that the cell apoptosis occurred after a NIR light exposure for 3 min. ICP results further indicated that the total amount of the A54-nanoshells attached on the surface of the cells and internalized by the cells at different times were very similar (between 25 and 28%). Although the amount

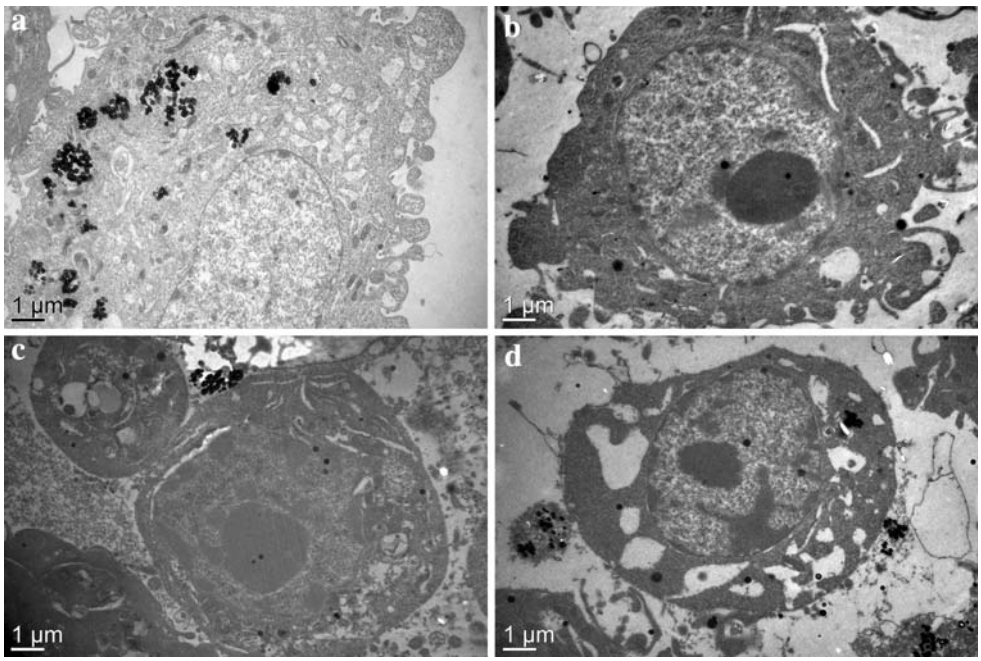

Fig. 7 TEM images of the liver cancer cells BEL-7404 incubated with the A54-nanoshells for 24 h and treated with a NIR light for different time: **a** 0 min; **b** 1 min; **c** 3 min; **d** 5 min. Representative images from two experiments were shown

of the A54-nanoshells internalized by the cell increased with time, it was relatively smaller than that on the cell surface and hence the nanoshells on the cell surface would contribute more of the thermal energy to destroy the cells.

4 Conclusions

Small peptides, A54, with liver cancer cell targeting ability were covalently linked to the gold nanoshells through amino acids, Cysteines. The A54-nanoshells were characterized by FT-IR, Raman, UV–vis and TEM. DLS results proved that the A54-nanoshells were more stable in water or in the culture medium, RMPI 1640. TGA results showed that about 3.0×10^3 peptides were attached to each gold nanoshell. The low cytotoxic activity of the A54-nanoshells was confirmed by MTT and FCM analyses. In vitro study of the targeting properties of the A54-nanoshells revealed that nanoshells functionalized with this small peptide A54 can significantly increase the efficiency of cancer cell death in the NIR photothermal treatment due to the specific binding (targeting) between the A54-nanoshells and the liver cancer cells, BEL-7404 and BEL-7402. In a TEM study of the death of the cancer cell, after incubation with the A54-nanoshells and irradiation with a NIR light, dramatic cell morphology changes as irradiation time increase was clearly demonstrated. Flow cytometry revealed the cell apoptosis after the cancer cell was exposed to a NIR light for a few minutes. Our results show that the A54-nanoshells can be used as promising agents for the selective treatment of liver cancers in the photothermal ablation therapy. Current efforts on the study of the immunogenicity and the use of the A54-nanoshells to treat the hepatocarcinoma in vivo by photothermal therapy are undergoing in our laboratories.

Acknowledgment This work was supported by the Science and Technology Commission of Shanghai Municipality under the Grant Nos. 0752nm022, 07ZR14034 and 0852nm03700.

References

1. Pisani P, Parkin DM, Bray F, Ferlay J. Estimates of the worldwide mortality from 25 cancers in 1990. Int J Cancer. 1999;83:18–29.
2. Sachdeva MS. Drug targeting systems for cancer chemotherapy. Expert Opin Invest Drugs. 1998;7:1849–64.
3. Torchilin VP. Drug targeting. Eur J Pharm Sci. 2000;11:81–91.
4. Hirsch LR, Stafford RJ, Bankson JA, Sershen SR, Halas NJ. Nanoshell-mediated near-infrared thermal therapy of tumors under magnetic resonance guidance. Proc Natl Acad Sci. 2003;100:13549–54.
5. Gobin AM, Lee MH, Halas NJ, James WD. Near-infrared resonant nanoshells for combined optical imaging and photothermal cancer therapy. Nano Lett. 2007;7:1929–34.
6. Maltzahn G, Park J-H, Agrawal A, Bandaru NK, Das SK, Sailor MJ, et al. Computationally cuided photothermal tumor therapy using long-circulating gold nanorod antennas. Cancer Res. 2009;69:3892–9.
7. Lal S, Clare SE, Halas NJ. Nanoshell-enabled photothermal cancer therapy: impending clinical inpact. Acc Chem Res. 2008;41:1842–51.
8. Loo C, Hirsch L, Lee MH, Chang E, West J, Halas NJ, et al. Gold nanoshell bioconjugates for molecular imaging in living cells. Opt Lett. 2005;30:1012–4.
9. Oldenburg SJ, Jackson JB, Westcott SL, Halas NJ. Infrared extinction properties of gold nanoshells. Appl Phys Lett. 1999;111:2897–9.

10. Hirsch LR, Gobin AM, Lowery AR, Drezek RA, Halas NJ, West JL. Metal nanoshells. Ann Biomed Eng. 2006;34:15–22.
11. Gobin AM, O'Neal DP, Watkins DM, Halas NJ, Drezek RA, West JL. Near infrared laser-tissue welding using nanoshells as an exogenous absorber. Lasers Surg Med. 2005;9999:1–7.
12. O'Neal DP, Hirsch LR, Halas NJ, Payne JD, West JL. Photothermal tumor ablation in mice using near infrared-absorbing nanoparticles. Cancer Lett. 2004;209:171–6.
13. Hashizume H, Baluk P, Morikawa S, McLean JW. Openings between defective endothelial cells explain tumor vessel leakiness. Am J Pathol. 2000;156:1363–80.
14. Loo C, Lowery A, Halas NJ, West JL, Drezek R. Immunotargeted nanoshells for integrated cancer imaging and therapy. Nano Lett. 2005;5:709–11.
15. Lowery AR, Gobin AM, Day ES, Halas NJ, West JL. Immunonanoshells for targeted photothermal ablation of tumor cells. Int J Nanomed. 2006;1:149–54.
16. Lin AWH, Lewinski NA, West JL. Optically tunable nanoparticle contrast agents for early cancer detection: model-based analysis of gold nanoshells. J Biomed Opt. 2005;10:064035-1-10.
17. Diagaradjane P, Shetty A, Wang JC, Elliott AM, Schwartz J, Shentu S, et al. Modulation of in vivo tumor radiation response via gold nanoshell-mediated vascular-focused hyperthermia: characterizing an integrated antihypoxic and localized vascular disrupting targeting strategy. Nano Lett. 2008;8:1492–500.
18. Dixit V, Bossche JV, Sherman DM, Thompson DH. Synthesis and grafting of thioctic acid-PEG-folate conjugates onto Au nanoparticles for selective targeting of folate receptor-positive tumor cells. Bioconjugate Chem. 2006;17:603–9.
19. Wang SN, Deng YH, Xu H, Wu HB, Qiu YK, Chen DW. Synthesis of a novel galactosylated lipid and its application to the hepatocyte-selective targeting of liposomal doxorubicin. Eur J Pharma Biopharma. 2006;62:32–8.
20. Otte A, Mueller-Brand J, Dellas S, Nitzsche EU, Herrmann R, Maecke HR. Yttrium-90-labelled somatostatin-analogue for cancer treatment. Lancet. 1998;351:417–8.
21. Yang Y, Jiang J-S, Du B, Gan Z-F, Qian M, Zhang P. Preparation and properties of a novel drug delivery system with both magnetic and biomolecular targeting. J Mater Sci Mater Med. 2009;20:301–7.
22. Pham T, Jackson JB, Halas NJ, Lee TR. Preparation and characterization of gold nanoshells coated with self-assembled monolayers. Langmuir. 2002;18:4915–20.
23. Stöber W, Fink A. Controlled growth of monodisperse silica spheres in the micron size range. J Colloid Interface Sci. 1968;26:62–9.
24. Duff DG, Baiker A. A new hydrosol of gold clusters. 1. Formation and particle size variation. Langmuir. 1993;9:2301–9.
25. Kong G, Braun RD, Dewhirst MW. Hyperthermia enables tumor-specific nanoparticle delivery: effect of particle size. Cancer Res. 2000;60:4440–5.
26. Ishida O, Maruyama K, Sasaki K, Iwatsuru M. Size-dependent extravasation and interstitial localization of polyethyleneglycol liposomes in solid tumor-bearing mice. Int J Pharm. 1999; 190:49–56.
27. Hobbs SK, Monsky WL, Yuan F, Roberts WG, Griffith L, Torchilin VP, et al. Regulation of transport pathways in tumor vessels: role of tumor type and microenvironment. Proc Natl Acad Sci. 1998;95:4607–12.
28. Birnboim MH, Ma WP. Nonlinear optical properties of structured nanoparticle composites. Mater Res Soc Symp Proc. 1990;164:277–82.
29. Wang YJ, Zhu SG, Xun CF. Biochemistry. 3rd ed. Beijing, China: Higher Education Press; 2003.
30. Fuente JM, Berry CC, Riehle MO. Nanoparticle targeting at cells. Langmuir. 2006;22:3286–93.
31. Chen JY, Saeki F, Wiley BJ. Gold nanocages: bioconjugation and their potential use as optical imaging contrast agents. Nano Lett. 2005;5:473–7.
32. Young JK, Chong RP. Analysis of problematic complexing behavior of ferric chloride with N,N-dimethylformamide using combined techniques of FT-IR, XPS, and TGA/DTG. Inorg Chem. 2002;41:6211–6.
33. Carmen T, Bogdan G, Vasile IP, Víctor LF, André G, Michael UK. Investigation of the hydrophobization efficiency of terbium-exchanged BEA zeolites by means of FT-IR, TGA, physical adsorption, and time-resolved photoluminescence. Langmuir. 2007;23:6781–7.
34. Mosmann T. Rapid colorimetric assay for cellular growth and survival: application to proliferation and cytotoxicity assays. J Immunol Methods. 1983;65:55–63.
35. Sgouras D, Duncan R. Methods for the evaluation of biocompatibility of soluble synthetic polymers which have potential for biomedical use: 1-Use of the tetrazolium-based colorimetric assay (MTT) as a preliminary screen for evaluation ofin vitro cytotoxicity. J Mater Sci: Mater Med. 1990;1:67–8.
36. Homa J, Bzowska M, Klimek M, Plytycz B. Flow cytometric quantification of proliferating coelomocytes non-invasively retrieved from the earthworm, *Dendrobaena veneta*. Dev Comp Immunol. 2008;32:9–14.
37. Jin C, Bai L, Wu H, Tian F, Guo G. Radiosensitization of paclitaxel, etanidazole and paclitaxel+etanidazole nanoparticles on hypoxic human tumor cells in vitro. Biomaterials. 2007;28:3724–30.
38. Kah JCY, Wan RCY, Wong KY, Mhaisalkar S, Sheppard CJR, Olivo M. Combinatorial treatment of photothermal therapy using cold nanoshells with conventional photodynamic therapy to improve treatment efficacy: an in vitro study. Lasers Surg Med. 2008;40:584–9.
39. Haveman J, Hahn GM. The role of energy in dyperthermia-induced mammalian cell inactivation: a study of the effects of glucose starvation and an uncoupler of oxidative phosphorylation. J Cell Physiol. 1981;107:237–41.
40. Ishiguro K, Hatcho M, Miyoshi N, Fukuda M, Ueda K. Microfluorocytometric detection of nuclear DNA damage to cancer cells in squamous cell carcinoma after hyperthermia. J Dermatol. 1994;21:92–7.